University of Nebraska - Lincoln
DigitalCommons@University of Nebraska - Lincoln

Kenneth Bloom Publications | Research Papers in Physics and Astronomy

3-2-2006

Measurement of mass and width of the excited charmed meson states D_1^0 and D_2^{*0} at CDF

A. Abulencia
University of Illinois, Urbana, Illinois 61801, USA

Kenneth Bloom
University of Nebraska - Lincoln, kenbloom@unl.edu

CDF Collaboration

Follow this and additional works at: http://digitalcommons.unl.edu/physicsbloom

Part of the Physics Commons

Abulencia, A.; Bloom, Kenneth; and Collaboration, CDF, "Measurement of mass and width of the excited charmed meson states D_1^0 and D_2^{*0} at CDF" (2006). *Kenneth Bloom Publications.* Paper 173.
http://digitalcommons.unl.edu/physicsbloom/173

This Article is brought to you for free and open access by the Research Papers in Physics and Astronomy at DigitalCommons@University of Nebraska - Lincoln. It has been accepted for inclusion in Kenneth Bloom Publications by an authorized administrator of DigitalCommons@University of Nebraska - Lincoln.

Measurement of mass and width of the excited charmed meson states D_1^0 and D_2^{*0} at CDF

A. Abulencia,[23] D. Acosta,[17] J. Adelman,[13] T. Affolder,[10] T. Akimoto,[53] M. G. Albrow,[16] D. Ambrose,[16] S. Amerio,[42] D. Amidei,[33] A. Anastassov,[50] K. Anikeev,[16] A. Annovi,[44] J. Antos,[1] M. Aoki,[53] G. Apollinari,[16] J.-F. Arguin,[32] T. Arisawa,[55] A. Artikov,[14] W. Ashmanskas,[16] A. Attal,[8] F. Azfar,[41] P. Azzi-Bacchetta,[42] P. Azzurri,[44] N. Bacchetta,[42] H. Bachacou,[28] W. Badgett,[16] A. Barbaro-Galtieri,[28] V. E. Barnes,[46] B. A. Barnett,[24] S. Baroiant,[7] V. Bartsch,[30] G. Bauer,[31] F. Bedeschi,[44] S. Behari,[24] S. Belforte,[52] G. Bellettini,[44] J. Bellinger,[57] A. Belloni,[31] E. Ben-Haim,[16] D. Benjamin,[15] A. Beretvas,[16] J. Beringer,[28] T. Berry,[29] A. Bhatti,[48] M. Binkley,[16] D. Bisello,[42] M. Bishai,[16] R. E. Blair,[2] C. Blocker,[6] K. Bloom,[33] B. Blumenfeld,[24] A. Bocci,[48] A. Bodek,[47] V. Boisvert,[47] G. Bolla,[46] A. Bolshov,[31] D. Bortoletto,[46] J. Boudreau,[45] S. Bourov,[16] A. Boveia,[10] B. Brau,[10] C. Bromberg,[34] E. Brubaker,[13] J. Budagov,[14] H. S. Budd,[47] S. Budd,[23] K. Burkett,[16] G. Busetto,[42] P. Bussey,[20] K. L. Byrum,[2] S. Cabrera,[15] M. Campanelli,[19] M. Campbell,[33] F. Canelli,[8] A. Canepa,[46] D. Carlsmith,[57] R. Carosi,[44] S. Carron,[15] M. Casarsa,[52] A. Castro,[5] P. Catastini,[44] D. Cauz,[52] M. Cavalli-Sforza,[3] A. Cerri,[28] L. Cerrito,[41] S. H. Chang,[27] J. Chapman,[33] Y. C. Chen,[1] M. Chertok,[7] G. Chiarelli,[44] G. Chlachidze,[14] F. Chlebana,[16] I. Cho,[27] K. Cho,[27] D. Chokheli,[14] J. P. Chou,[21] P. H. Chu,[23] S. H. Chuang,[57] K. Chung,[12] W. H. Chung,[57] Y. S. Chung,[47] M. Ciljak,[44] C. I. Ciobanu,[23] M. A. Ciocci,[44] A. Clark,[19] D. Clark,[6] M. Coca,[15] A. Connolly,[28] M. E. Convery,[48] J. Conway,[7] B. Cooper,[30] K. Copic,[33] M. Cordelli,[18] G. Cortiana,[42] A. Cruz,[17] J. Cuevas,[11] R. Culbertson,[16] D. Cyr,[57] S. DaRonco,[42] S. D'Auria,[20] M. D'onofrio,[19] D. Dagenhart,[6] P. de Barbaro,[47] S. De Cecco,[49] A. Deisher,[28] G. De Lentdecker,[47] M. Dell'Orso,[44] S. Demers,[47] L. Demortier,[48] J. Deng,[15] M. Deninno,[5] D. De Pedis,[49] P. F. Derwent,[16] C. Dionisi,[49] J. Dittmann,[4] P. DiTuro,[50] C. Dörr,[25] A. Dominguez,[28] S. Donati,[44] M. Donega,[19] P. Dong,[8] J. Donini,[42] T. Dorigo,[42] S. Dube,[50] K. Ebina,[55] J. Efron,[38] J. Ehlers,[19] R. Erbacher,[7] D. Errede,[23] S. Errede,[23] R. Eusebi,[47] H. C. Fang,[28] S. Farrington,[29] I. Fedorko,[44] W. T. Fedorko,[13] R. G. Feild,[58] M. Feindt,[25] J. P. Fernandez,[46] R. Field,[17] G. Flanagan,[34] L. R. Flores-Castillo,[45] A. Foland,[21] S. Forrester,[7] G. W. Foster,[16] M. Franklin,[21] J. C. Freeman,[28] Y. Fujii,[26] I. Furic,[13] A. Gajjar,[29] M. Gallinaro,[48] J. Galyardt,[12] J. E. Garcia,[44] M. Garcia Sciverez,[28] A. F. Garfinkel,[46] C. Gay,[58] H. Gerberich,[23] E. Gerchtein,[12] D. Gerdes,[33] S. Giagu,[49] P. Giannetti,[44] A. Gibson,[28] K. Gibson,[12] C. Ginsburg,[16] K. Giolo,[46] M. Giordani,[52] M. Giunta,[44] G. Giurgiu,[12] V. Glagolev,[14] D. Glenzinski,[16] M. Gold,[36] N. Goldschmidt,[33] J. Goldstein,[41] G. Gomez,[11] G. Gomez-Ceballos,[11] M. Goncharov,[51] O. González,[46] I. Gorelov,[36] A. T. Goshaw,[15] Y. Gotra,[45] K. Goulianos,[48] A. Gresele,[42] M. Griffiths,[29] S. Grinstein,[21] C. Grosso-Pilcher,[13] U. Grundler,[23] J. Guimaraes da Costa,[21] C. Haber,[28] S. R. Hahn,[16] K. Hahn,[43] E. Halkiadakis,[47] A. Hamilton,[32] B.-Y. Han,[47] R. Handler,[57] F. Happacher,[18] K. Hara,[53] M. Hare,[54] S. Harper,[41] R. F. Harr,[56] R. M. Harris,[16] K. Hatakeyama,[48] J. Hauser,[8] C. Hays,[15] H. Hayward,[29] A. Heijboer,[43] B. Heinemann,[29] J. Heinrich,[43] M. Hennecke,[25] M. Herndon,[57] J. Heuser,[25] D. Hidas,[15] C. S. Hill,[10] D. Hirschbuehl,[25] A. Hocker,[16] A. Holloway,[21] S. Hou,[1] M. Houlden,[29] S.-C. Hsu,[9] B. T. Huffman,[41] R. E. Hughes,[38] J. Huston,[34] K. Ikado,[55] J. Incandela,[10] G. Introzzi,[44] M. Iori,[49] Y. Ishizawa,[53] A. Ivanov,[7] B. Iyutin,[31] E. James,[16] D. Jang,[50] B. Jayatilaka,[33] D. Jeans,[49] H. Jensen,[16] E. J. Jeon,[27] M. Jones,[46] K. K. Joo,[27] S. Y. Jun,[12] T. R. Junk,[23] T. Kamon,[51] J. Kang,[33] M. Karagoz-Unel,[37] P. E. Karchin,[56] Y. Kato,[40] Y. Kemp,[25] R. Kephart,[16] U. Kerzel,[25] V. Khotilovich,[51] B. Kilminster,[38] D. H. Kim,[27] H. S. Kim,[27] J. E. Kim,[27] M. J. Kim,[12] M. S. Kim,[27] S. B. Kim,[27] S. H. Kim,[53] Y. K. Kim,[13] M. Kirby,[15] L. Kirsch,[6] S. Klimenko,[17] M. Klute,[31] B. Knuteson,[31] B. R. Ko,[15] H. Kobayashi,[53] K. Kondo,[55] D. J. Kong,[27] J. Konigsberg,[17] K. Kordas,[32] A. Korytov,[17] A. V. Kotwal,[15] A. Kovalev,[43] J. Kraus,[23] I. Kravchenko,[31] M. Kreps,[25] A. Kreymer,[16] J. Kroll,[43] N. Krumnack,[4] M. Kruse,[15] V. Krutelyov,[51] S. E. Kuhlmann,[2] Y. Kusakabe,[55] S. Kwang,[13] A. T. Laasanen,[46] S. Lai,[32] S. Lami,[48] S. Lammel,[16] M. Lancaster,[30] R. L. Lander,[7] K. Lannon,[38] A. Lath,[50] G. Latino,[44] I. Lazzizzera,[42] C. Lecci,[25] T. LeCompte,[2] J. Lee,[27] J. Lee,[47] S. W. Lee,[51] R. Lefèvre,[3] N. Leonardo,[31] S. Leone,[44] S. Levy,[13] J. D. Lewis,[16] K. Li,[58] C. Lin,[58] C. S. Lin,[16] M. Lindgren,[16] E. Lipeles,[9] T. M. Liss,[23] A. Lister,[19] D. O. Litvintsev,[16] T. Liu,[16] Y. Liu,[19] N. S. Lockyer,[43] A. Loginov,[35] M. Loreti,[42] P. Loverre,[49] R.-S. Lu,[1] D. Lucchesi,[42] P. Lujan,[28] P. Lukens,[16] G. Lungu,[17] L. Lyons,[41] J. Lys,[28] R. Lysak,[1] E. Lytken,[46] P. Mack,[25] D. MacQueen,[32] R. Madrak,[16] K. Maeshima,[16] P. Maksimovic,[24] G. Manca,[29] F. Margaroli,[5] R. Marginean,[16] C. Marino,[23] A. Martin,[58] M. Martin,[24] V. Martin,[37] M. Martínez,[3] T. Maruyama,[53] H. Matsunaga,[53] M. E. Mattson,[56] R. Mazini,[32] P. Mazzanti,[5] K. S. McFarland,[47] D. McGivern,[30] P. McIntyre,[51] P. McNamara,[50] R. McNulty,[29] A. Mehta,[29] S. Menzemer,[31] A. Menzione,[44] P. Merkel,[46] C. Mesropian,[48] A. Messina,[49] M. von der Mey,[8] T. Miao,[16] N. Miladinovic,[6] J. Miles,[31] R. Miller,[34] J. S. Miller,[33] C. Mills,[10] M. Milnik,[25] R. Miquel,[28] S. Miscetti,[18] G. Mitselmakher,[17] A. Miyamoto,[26] N. Moggi,[5] B. Mohr,[8] R. Moore,[16] M. Morello,[44] P. Movilla Fernandez,[28] J. Mülmenstädt,[28] A. Mukherjee,[16] M. Mulhearn,[31] Th. Muller,[25] R. Mumford,[24] P. Murat,[16] J. Nachtman,[16] S. Nahn,[58] I. Nakano,[39] A. Napier,[54] D. Naumov,[36] V. Necula,[17] C. Neu,[43] M. S. Neubauer,[9] J. Nielsen,[28] T. Nigmanov,[45] L. Nodulman,[2]

 © 2006 The American Physical Society

O. Norniella,[3] T. Ogawa,[55] S. H. Oh,[15] Y. D. Oh,[27] T. Okusawa,[40] R. Oldeman,[29] R. Orava,[22] K. Osterberg,[22] C. Pagliarone,[44] E. Palencia,[11] R. Paoletti,[44] V. Papadimitriou,[16] A. Papikonomou,[25] A. A. Paramonov,[13] B. Parks,[38] S. Pashapour,[32] J. Patrick,[16] G. Pauletta,[52] M. Paulini,[12] C. Paus,[31] D. E. Pellett,[7] A. Penzo,[52] T. J. Phillips,[15] G. Piacentino,[44] J. Piedra,[11] K. Pitts,[23] C. Plager,[8] L. Pondrom,[57] G. Pope,[45] X. Portell,[3] O. Poukhov,[14] N. Pounder,[41] F. Prakoshyn,[14] A. Pronko,[16] J. Proudfoot,[2] F. Ptohos,[18] G. Punzi,[44] J. Pursley,[24] J. Rademacker,[41] A. Rahaman,[45] A. Rakitin,[31] S. Rappoccio,[21] F. Ratnikov,[50] B. Reisert,[16] V. Rekovic,[36] N. van Remortel,[22] P. Renton,[41] M. Rescigno,[49] S. Richter,[25] F. Rimondi,[5] K. Rinnert,[25] L. Ristori,[44] W. J. Robertson,[15] A. Robson,[20] T. Rodrigo,[11] E. Rogers,[23] S. Rolli,[54] R. Roser,[16] M. Rossi,[52] R. Rossin,[17] C. Rott,[46] A. Ruiz,[11] J. Russ,[12] V. Rusu,[13] D. Ryan,[54] H. Saarikko,[22] S. Sabik,[32] A. Safonov,[7] W. K. Sakumoto,[47] G. Salamanna,[49] O. Salto,[3] D. Saltzberg,[8] C. Sanchez,[3] L. Santi,[52] S. Sarkar,[49] K. Sato,[53] P. Savard,[32] A. Savoy-Navarro,[16] T. Scheidle,[25] P. Schlabach,[16] E. E. Schmidt,[16] M. P. Schmidt,[58] M. Schmitt,[37] T. Schwarz,[33] L. Scodellaro,[11] A. L. Scott,[10] A. Scribano,[44] F. Scuri,[44] A. Sedov,[46] S. Seidel,[36] Y. Seiya,[40] A. Semenov,[14] F. Semeria,[5] L. Sexton-Kennedy,[16] I. Sfiligoi,[18] M. D. Shapiro,[28] T. Shears,[29] P. F. Shepard,[45] D. Sherman,[21] M. Shimojima,[53] M. Shochet,[13] Y. Shon,[57] I. Shreyber,[35] A. Sidoti,[44] P. Sinervo,[32] A. Sisakyan,[14] J. Sjolin,[41] A. Skiba,[25] A. J. Slaughter,[16] K. Sliwa,[54] D. Smirnov,[36] J. R. Smith,[7] F. D. Snider,[16] R. Snihur,[32] M. Soderberg,[33] A. Soha,[7] S. Somalwar,[50] V. Sorin,[34] J. Spalding,[16] F. Spinella,[44] P. Squillacioti,[44] M. Stanitzki,[58] A. Staveris-Polykalas,[44] R. St. Denis,[20] B. Stelzer,[8] O. Stelzer-Chilton,[32] D. Stentz,[37] J. Strologas,[36] D. Stuart,[10] J. S. Suh,[27] A. Sukhanov,[17] K. Sumorok,[31] H. Sun,[54] T. Suzuki,[53] A. Taffard,[23] R. Tafirout,[32] R. Takashima,[39] Y. Takeuchi,[53] K. Takikawa,[53] M. Tanaka,[2] R. Tanaka,[39] M. Tecchio,[33] P. K. Teng,[1] K. Terashi,[48] S. Tether,[31] J. Thom,[16] A. S. Thompson,[20] E. Thomson,[43] P. Tipton,[47] V. Tiwari,[12] S. Tkaczyk,[16] D. Toback,[51] K. Tollefson,[34] T. Tomura,[53] D. Tonelli,[44] M. Tönnesmann,[34] S. Torre,[44] D. Torretta,[16] S. Tourneur,[16] W. Trischuk,[32] R. Tsuchiya,[55] S. Tsuno,[39] N. Turini,[44] F. Ukegawa,[53] T. Unverhau,[20] S. Uozumi,[53] D. Usynin,[43] L. Vacavant,[28] A. Vaiciulis,[47] S. Vallecorsa,[19] A. Varganov,[33] E. Vataga,[36] G. Velev,[16] G. Veramendi,[23] V. Veszpremi,[46] T. Vickey,[23] R. Vidal,[16] I. Vila,[11] R. Vilar,[11] I. Vollrath,[32] I. Volobouev,[28] F. Würthwein,[9] P. Wagner,[51] R. G. Wagner,[2] R. L. Wagner,[16] W. Wagner,[25] R. Wallny,[8] T. Walter,[25] Z. Wan,[50] M. J. Wang,[1] S. M. Wang,[17] A. Warburton,[32] B. Ward,[20] S. Waschke,[20] D. Waters,[30] T. Watts,[50] M. Weber,[28] W. C. Wester III,[16] B. Whitehouse,[54] D. Whiteson,[43] A. B. Wicklund,[2] E. Wicklund,[16] H. H. Williams,[43] P. Wilson,[16] B. L. Winer,[38] P. Wittich,[43] S. Wolbers,[16] C. Wolfe,[13] S. Worm,[50] T. Wright,[33] X. Wu,[19] S. M. Wynne,[29] A. Yagil,[16] K. Yamamoto,[40] J. Yamaoka,[50] Y. Yamashita,[39] C. Yang,[58] U. K. Yang,[13] W. M. Yao,[28] G. P. Yeh,[16] J. Yoh,[16] K. Yorita,[13] T. Yoshida,[40] I. Yu,[27] S. S. Yu,[43] J. C. Yun,[16] L. Zanello,[49] A. Zanetti,[52] I. Zaw,[21] F. Zetti,[44] X. Zhang,[23] J. Zhou,[50] and S. Zucchelli[5]

(CDF Collaboration)

[1]*Institute of Physics, Academia Sinica, Taipei, Taiwan 11529, Republic of China*
[2]*Argonne National Laboratory, Argonne, Illinois 60439, USA*
[3]*Institut de Fisica d'Altes Energies, Universitat Autonoma de Barcelona, E-08193, Bellaterra (Barcelona), Spain*
[4]*Baylor University, Waco, Texas 76798, USA*
[5]*Istituto Nazionale di Fisica Nucleare, University of Bologna, I-40127 Bologna, Italy*
[6]*Brandeis University, Waltham, Massachusetts 02254, USA*
[7]*University of California, Davis, Davis, California 95616, USA*
[8]*University of California, Los Angeles, Los Angeles, California 90024, USA*
[9]*University of California, San Diego, La Jolla, California 92093, USA*
[10]*University of California, Santa Barbara, Santa Barbara, California 93106, USA*
[11]*Instituto de Fisica de Cantabria, CSIC-University of Cantabria, 39005 Santander, Spain*
[12]*Carnegie Mellon University, Pittsburgh, Pennsylvania 15213, USA*
[13]*Enrico Fermi Institute, University of Chicago, Chicago, Illinois 60637, USA*
[14]*Joint Institute for Nuclear Research, RU-141980 Dubna, Russia*
[15]*Duke University, Durham, North Carolina 27708*
[16]*Fermi National Accelerator Laboratory, Batavia, Illinois 60510, USA*
[17]*University of Florida, Gainesville, Florida 32611, USA*
[18]*Laboratori Nazionali di Frascati, Istituto Nazionale di Fisica Nucleare, I-00044 Frascati, Italy*
[19]*University of Geneva, CH-1211 Geneva 4, Switzerland*
[20]*Glasgow University, Glasgow G12 8QQ, United Kingdom*
[21]*Harvard University, Cambridge, Massachusetts 02138, USA*
[22]*Division of High Energy Physics, Department of Physics, University of Helsinki and Helsinki Institute of Physics, FIN-00014, Helsinki, Finland*

[23]University of Illinois, Urbana, Illinois 61801, USA
[24]The Johns Hopkins University, Baltimore, Maryland 21218, USA
[25]Institut für Experimentelle Kernphysik, Universität Karlsruhe, 76128 Karlsruhe, Germany
[26]High Energy Accelerator Research Organization (KEK), Tsukuba, Ibaraki 305, Japan
[27]Center for High Energy Physics, Kyungpook National University, Taegu 702-701;
Seoul National University, Seoul 151-742;
and SungKyunKwan University, Suwon 440-746, Korea
[28]Ernest Orlando Lawrence Berkeley National Laboratory, Berkeley, California 94720, USA
[29]University of Liverpool, Liverpool L69 7ZE, United Kingdom
[30]University College London, London WC1E 6BT, United Kingdom
[31]Massachusetts Institute of Technology, Cambridge, Massachusetts 02139, USA
[32]Institute of Particle Physics: McGill University, Montréal, Canada H3A 2T8;
and University of Toronto, Toronto, Canada M5S 1A7
[33]University of Michigan, Ann Arbor, Michigan 48109, USA
[34]Michigan State University, East Lansing, Michigan 48824, USA
[35]Institution for Theoretical and Experimental Physics, ITEP, Moscow 117259, Russia
[36]University of New Mexico, Albuquerque, New Mexico 87131, USA
[37]Northwestern University, Evanston, Illinois 60208, USA
[38]The Ohio State University, Columbus, Ohio 43210, USA
[39]Okayama University, Okayama 700-8530, Japan
[40]Osaka City University, Osaka 588, Japan
[41]University of Oxford, Oxford OX1 3RH, United Kingdom
[42]University of Padova, Istituto Nazionale di Fisica Nucleare, Sezione di Padova-Trento, I-35131 Padova, Italy
[43]University of Pennsylvania, Philadelphia, Pennsylvania 19104, USA
[44]Istituto Nazionale di Fisica Nucleare Pisa, Universities of Pisa, Siena
and Scuola Normale Superiore, I-56127 Pisa, Italy
[45]University of Pittsburgh, Pittsburgh, Pennsylvania 15260, USA
[46]Purdue University, West Lafayette, Indiana 47907, USA
[47]University of Rochester, Rochester, New York 14627, USA
[48]The Rockefeller University, New York, New York 10021, USA
[49]Istituto Nazionale di Fisica Nucleare, Sezione di Roma 1, University di Roma "La Sapienza," I-00185 Roma, Italy
[50]Rutgers University, Piscataway, New Jersey 08855, USA
[51]Texas A&M University, College Station, Texas 77843, USA
[52]Istituto Nazionale di Fisica Nucleare, University of Trieste/Udine, Italy
[53]University of Tsukuba, Tsukuba, Ibaraki 305, Japan
[54]Tufts University, Medford, Massachusetts 02155, USA
[55]Waseda University, Tokyo 169, Japan
[56]Wayne State University, Detroit, Michigan 48201, USA
[57]University of Wisconsin, Madison, Wisconsin 53706, USA
[58]Yale University, New Haven, Connecticut 06520, USA
(Received 27 December 2005; published 6 March 2006)

We report on precision measurements of the masses and widths of the narrow, orbitally excited states D_1^0 and D_2^{*0} using the CDF II detector at the Fermilab Tevatron. Both states (collectively called D^{**}) are reconstructed in the decay channel $D^{**} \to D^{*+}\pi^-$. The D_2^{*0} is also reconstructed in the $D^{**} \to D^+\pi^-$ channel. Using a data set with an integrated luminosity of 210 pb^{-1}, the measured masses and widths for the D_1^0 are $2421.7 \pm 0.7 \pm 0.6$ MeV$/c^2$ and $20.0 \pm 1.7 \pm 1.3$ MeV$/c^2$ respectively, while for the D_2^{*0} they are $2463.3 \pm 0.6 \pm 0.8$ MeV$/c^2$ and $49.2 \pm 2.3 \pm 1.2$ MeV$/c^2$. These values are currently the single best measurements available.

DOI: 10.1103/PhysRevD.73.051104 PACS numbers: 14.40.Lb, 12.40.Yx

The orbitally excited charmed meson states, collectively referred to as D^{**}, are P-wave excitations of the quark-antiquark system involving one charm and one light quark. If we write the total angular momentum as $\vec{J} = \vec{j}_q + \vec{s}_Q$; $\vec{j}_q = \vec{s}_q + \vec{L}$, where $\vec{L}$ is the orbital angular momentum and $Q(q)$ denotes the charm (light) quark, then in the heavy-quark limit $m_Q \gg \Lambda_{\rm QCD}$ the spin of the charm quark $\vec{s}_Q$ decouples from the other degrees of freedom. In that limit, the four P-wave states can be separated into mass degenerate pairs: $j_q = 1/2$ ($J^P = 0^+, 1^+$) and $j_q = 3/2$ ($J^P = 1^+, 2^+$). Heavy quark symmetry [1] provides a systematic treatment of the m_Q-dependent "hyperfine" splittings within each doublet, as well as the average mass splittings between doublets, as illustrated in Fig. 1.

The D_1^0 and D_2^{*0} states, which form the $j_q = 3/2$ doublet, are expected to decay into final states $D^*\pi$, with an

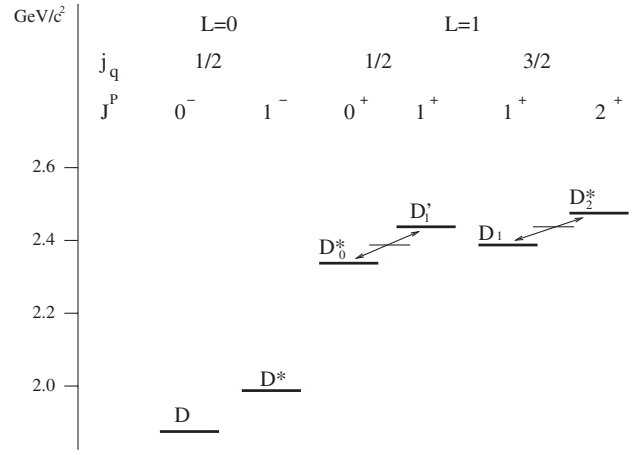

FIG. 1. The mass ordering of the $L = 0$ and $L = 1$ D-meson system. The arrows show the hyperfine splitting of the P-wave $j_q = 1/2$ and $j_q = 3/2$ states. Properties of the broad P-wave $j_q = 1/2$ states are not well established.

overall D-wave configuration, whereas the $j_q = 1/2$ states D_0^{*0} and $D_1'0'$ are expected to decay in an overall S-wave configuration. Thus the $j_q = 3/2$ states are expected to have narrow decay widths, comparable to their mass splitting [2], while the $j_q = 1/2$ states are expected to be much broader. Recent theory estimations give the mass values of the two $j_q = 3/2$ states [3–8].

These narrow orbitally excited charmed mesons have been observed by several experiments [9–16]. In principle, given the large charm cross section at the Tevatron $p\bar{p}$ collider, very high statistics samples can be collected for precision measurements of the properties of these states. However, at the trigger level it is difficult to separate low-mass fully hadronic D-meson decays from the overwhelming QCD background. The CDF II detector overcomes this obstacle with a novel two-track trigger, which selects long-lived charged hadrons from secondary vertices, thus suppressing prompt charged hadrons from the QCD background. The data set for this analysis, based on the vertex trigger, was taken between March 2001 and November 2003, corresponding to an integrated luminosity of 210 pb^{-1}. This sample is ideal for studies of charm-particle decays into two or more hadrons. In this analysis, both the D_1^0 and D_2^{*0} states have been observed in the $D^{*+}\pi^-$ channel, followed by the decay $D^{*+} \to D^0\pi^+$ and $D^0 \to K^-\pi^+$. The D_2^{*0} state has also been observed in the $D^+\pi^-$ channel (followed by $D^+ \to K^-\pi^+\pi^+$), where the corresponding D_1^0 decay is forbidden by parity and angular momentum conservation. Charge-conjugate decay modes are included in the analysis.

A description of CDF can be found in Ref. [17]; here only the pertinent detector components are described. This measurement uses tracks measured in the pseudorapidity range $|\eta| < 1.1$ [18], reconstructed by a silicon microstrip vertex detector (SVXII) [19] and the central outer tracker (COT) [20], both in a 1.4 T solenoidal magnetic field. The SVXII consists of double-sided sensors arranged in five cylindrical layers at radii between 2.5 and 10.6 cm, each providing an r-ϕ position measurement with a precision of ≈ 10 μm. The COT is an open-cell drift chamber with 96 layers of sense wires, grouped into 8 superlayers of alternating axial and 2° stereo readout, and providing track measurements between 40 and 137 cm in radius.

CDF collects events with a three-level trigger system. At level 1, two oppositely charged tracks are reconstructed in the COT by the extremely fast tracker (XFT) [21] and are required to have a transverse momentum $p_T \geq 2$ GeV/c each, and $p_{T1} + p_{T2} \geq 5.5$ GeV/c. At level 2, the silicon vertex tracker [22] associates SVXII r-ϕ position measurements with XFT tracks, providing a precise measurement of the track impact parameter (d_0), the distance of closest approach of the track trajectory to the beam axis in the transverse plane. Decays of long-lived particles are identified by requiring two tracks with 120 $\mu\text{m} \leq d_0 \leq$ 1.0 mm, an opening angle between the two tracks satisfying $2° \leq |\Delta\phi| \leq 90°$, and $L_{xy} > 200$ μm, where L_{xy} is the transverse distance from the beam axis to the two-track intersection projected along the total transverse momentum of the track pair. A complete event reconstruction of $D^0 \to K^-\pi^+$ is performed at level 3, where the level 1 and level 2 trigger requirements are confirmed.

The narrow width and small mass difference between the D^{**} states require stringent tracking calibration to achieve adequate mass resolution. The calibration procedure is done in two steps. The first step is to determine the error matrix for the COT track parameters, accounting for multiple scattering inside the COT volume. These uncertainties depend on the COT material description and hit resolution in the drift model. The error matrix is computed using simulated $J/\psi \to \mu^+\mu^-$ decays, by analyzing pull distributions of the five helix parameters between generated and reconstructed muon tracks. Maximum likelihood fits are performed in bins of p_T^2 of the J/ψ to derive the p_T-dependent rescaling factors. The second step is similar to that used in B mass measurements at CDF [23], but with improved energy loss calculations. We first use photon conversions to electron-positron pairs to determine the radiation length distribution of the inner detector material and then tune the energy loss parameters using the reconstructed J/ψ mass as a calibration. For this tuning we describe the detector as a series of cylindrical layers of different materials; in each layer we calculate the average dE/dx energy loss in the traversed medium and then refit the track parameters. The calibration uses the $J/\psi \to \mu^+\mu^-$ decays from data to iteratively adjust the material composition and thickness of each layer for different regions in z, until the J/ψ mass dependence on the transverse momentum is negligible. Finally, the absolute mass scale is reached by adjusting the magnetic field by 0.1% to set the value of the J/ψ mass to the world average value [24].

TABLE I. Summary of mass measurements used to validate the tracker calibration.

Meson	Decay mode	Slope ($\mathrm{MeV}/c^2/\mathrm{GeV}/c$)	$m - m_{\mathrm{PDG}}$ (MeV/c^2)
K_s^0	$\pi^+\pi^-$	-0.07 ± 0.16	-0.042 ± 0.086
$B^\pm$	$J/\psi K^\pm$	0.11 ± 0.06	-0.27 ± 1.037
J/ψ	$\mu^+\mu^-$	-0.006 ± 0.01	0 ± 0.45
$\Upsilon(1S)$	$\mu^+\mu^-$	-0.16 ± 0.21	-0.7 ± 1.9
D^0	$K^-\pi^+$	$(-9 \pm 6) \times 10^{-6}$	0.1 ± 0.55

Figure 2(a) shows the J/ψ mass versus p_T before and after calibration, where the slope changes from $0.50 \pm 0.03\ \mathrm{MeV}/c^2$ per GeV/c to $0.006 \pm 0.010\ \mathrm{MeV}/c^2$ per GeV/c and the mean corresponds to the world average J/ψ mass.

The tracking calibration has been cross-checked with several other particle samples which populate different mass ranges or different decay topologies, such as K_S^0, $\Upsilon(1S)$, $B^\pm$ (to check for charge asymmetry biases) and D^0. For all cases the masses agree well with the world averages, and the charge asymmetry was found to be negligible. The results of these tests are summarized in Table I. Figure 2(b) illustrates the results for the D^0, of particular relevance for this analysis.

Events considered in this analysis are required to have at least four tracks with total charge zero, out of which two are consistent with the trigger requirements ($p_T > 2\ \mathrm{GeV}/c$ and $|d_0| > 100\ \mu\mathrm{m}$). For the first channel ($D^{**} \to D^{*+}\pi^-$, followed by $D^{*+} \to D^0\pi^+$ and $D^0 \to K^-\pi^+$), these "trigger tracks" are required to have an invariant mass within $24\ \mathrm{MeV}/c^2$ of the D^0 mass of $1864.5\ \mathrm{MeV}/c^2$ [24]. Particles are assigned in turn the K and π masses, and all $K\pi$ combinations falling within the mass window are retained, to avoid any bias in the D^0 mass. This D^0 candidate is associated with another track with $p_T > 400\ \mathrm{MeV}/c$ to form a D^{*+} candidate, with the requirement that the mass difference between the D^{*+} and the D^0 be smaller than $147\ \mathrm{MeV}/c^2$. In addition, to reduce both background and misassignment of the K and π masses, the third track is required to have the same charge as the candidate pion track, as expected from leading order D^{*+} decays. Finally, the D^{*+} is associated with a negative track with $p_T > 400\ \mathrm{MeV}/c$, to form a four-track D^{**} candidate. For the second channel ($D_2^{*0} \to D^+\pi^-$, followed by $D^+ \to K^-\pi^+\pi^+$), no mass window is required for the trigger tracks. The D^+ candidate is constructed from three tracks with a mass and charge assignment compatible with being a $K^-\pi^+\pi^+$ system; two of these tracks must satisfy the trigger requirements, while the third must have $p_T > 800\ \mathrm{MeV}/c$. We first ensure that all three tracks originate from a common vertex which is well separated from the primary vertex, by requiring the χ^2 from a 3-dimensional fit to the three tracks to be smaller than 12, and have an associated $L_{xy} > 1$ mm. Then, D^+ candidates are defined as three-track systems with invariant mass between 1.85 and $1.89\ \mathrm{GeV}/c^2$. Finally, to obtain a neutral D^{**} candidate, the three tracks are combined with a fourth, of opposite charge with respect to the sum of the first three. The two D^{**} resonances are analyzed in terms of the invariant mass difference between the four-track and the three-track system, which is crucial to separate the resonances from the background. Figures 3 and 4 show the results for the D^{**} resonances in the two decay channels.

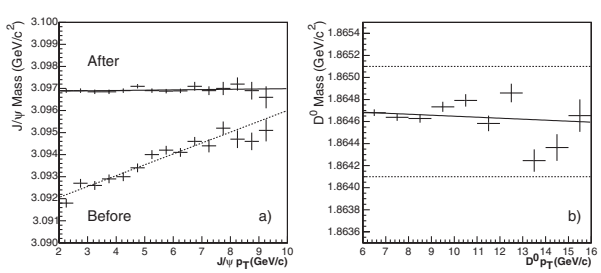

FIG. 2. (a) The J/ψ mass as a function of p_T, before (dashed) and after (solid) tracking calibration. The slope is reduced from 0.50 ± 0.03 to $0.006 \pm 0.010\ \mathrm{MeV}/c^2$ per GeV/c. (b) The D^0 mass as a function of p_T, after calibration. The dashed lines indicate the world average 1σ error band of $\sim 1\ \mathrm{MeV}/c^2$.

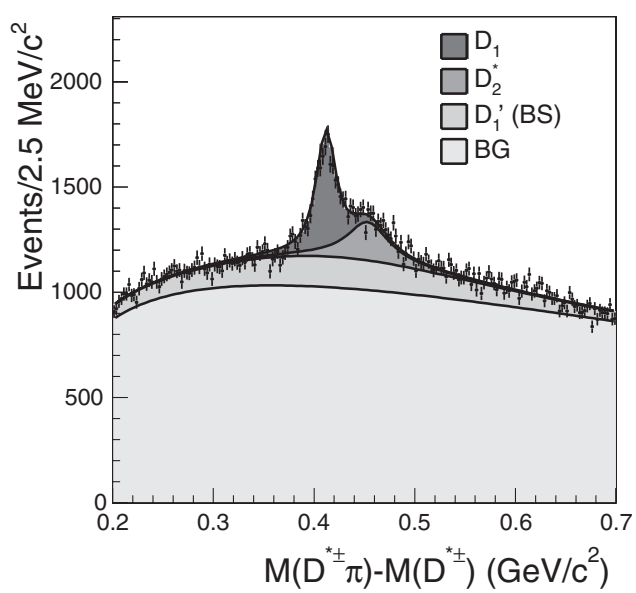

FIG. 3. Invariant mass difference between $D^*\pi$ system and the D^*. The points represent the data, and lines represent the projection of the fit results for the individual components described in the text.

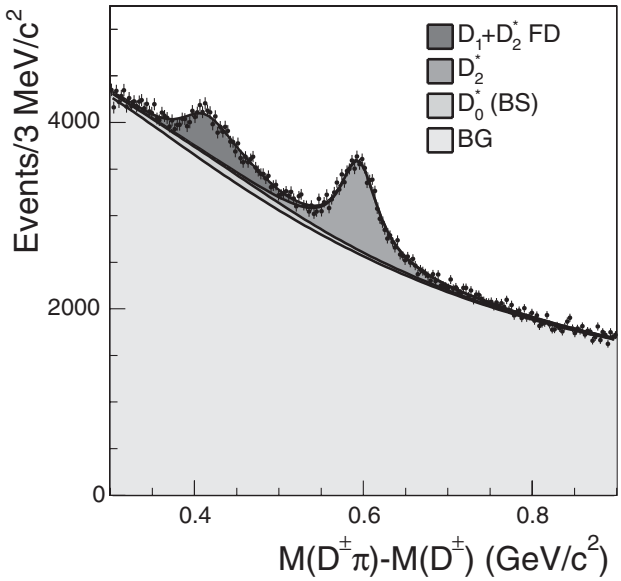

FIG. 4. Invariant mass difference between the $D^+\pi^-$ system and the D^+, with the same definitions as Fig. 3.

In Fig. 3, signals from the D_1^0 at 0.40 GeV/c^2 and the D_2^{*0} at 0.46 GeV/c^2 are clearly visible above the combinatorial background. Because of the unknown shape of the combinatorial background it is not possible with these data to derive with sufficient confidence the properties, or even the existence of the broad state (BS) $D_1^{0'}$ (the 1^+ component of the $j_q = 1/2$ doublet) from our data. Since a state with width around 200 MeV/c^2 is suggested by a Belle measurement [15] its potential effect is included as a systematic error.

The distribution of the mass difference in Fig. 4 presents two features: a broad peak around 0.4 GeV/c^2, and a narrow pronounced peak around 0.6 GeV/c^2. The broad peak is due to the feed-down decays of the type $D^{**} \to D^{*+}\pi^-$ accessible for both D_1^0 and D_2^{*0}, followed by $D^{*+} \to D^+\pi^0$, where the π^0 is not observed. Similar to the $D_1^{0'}$ in Fig. 3, part of this peak could be due to a broad neutral D_0^{*0} state with a mass around 2410 MeV/c^2 and width of about 250 MeV/c^2, as reported by FOCUS [11]. The peak around 0.6 GeV/c^2 is the main D_2^{*0} signal.

A simultaneous binned likelihood fit to both histograms in Figs. 3 and 4 is used to extract the mass and width for the D_1^0 and the D_2^{*0}. The likelihood function consists of:

(i) a signal term for each narrow state in the D^{*+} channel, and only a D_2^{*0} term in the D^+ channel. These terms are a convolution of a nonrelativistic Breit-Wigner (BW) distribution with a resolution histogram taken from Monte Carlo simulation, and depends on the amplitudes $A_{1,2}$, the mass differences with respect to the three-track states $M_{1,2}$ and widths $\Gamma_{1,2}$. The D_2^{*0} widths are common for the two channels. The likelihood component is

$$f_{D_{1,2}}(\Delta m) = A_{1,2} \times \mathrm{BW}(\Delta m, M_{1,2}, \Gamma_{1,2}) \otimes \text{Resolution}.$$

The D_2^{*0} masses in the two channels are connected by using the world average value for the mass difference between D^{*+} and D^*.

(ii) a background (BG) term for each histogram with free parameters α, β, γ, and δ (set to zero for the first channel), of the form

$$f_{\mathrm{BG}}(\Delta m) = \alpha(\Delta m - m_\pi)^\beta e^{-\gamma(\Delta m - m_\pi)} + \delta.$$

(iii) a broad state (BS) term for each histogram, modeled as a Breit-Wigner function similar to that of the narrow resonances, but convoluted with a Gaussian whose width is taken from simulation

$$f_{\mathrm{BS}}(\Delta m) = A_{\mathrm{BS}} \times \mathrm{BW}(\Delta m, M_{\mathrm{BS}}, \Gamma_{\mathrm{BS}}) \otimes \text{Resolution}.$$

(iv) a feed-down (FD) term for decays of D_1^0 and D_2^{*0} to $D\pi^0\pi$, where the π^0 is lost and a smaller mass is reconstructed. The only additional free parameter is a common scale factor relative to the amplitudes of the $D^*\pi$ channel, since the D_1^0 and D_2^{*0} masses and widths are the same. The shift and resolution are taken from Monte Carlo.

Overall we have seven parameters for the narrow resonances (amplitude, mass and width for each resonance, plus the D_2^{*0} yield in the second channel), seven for background modeling (one parameter is set to zero in the first channel), two amplitudes for broad states and one feed-down normalization, for a total of 17 parameters. If the mass and width of one or two broad states are left floating, we can have up to 19 or 21 parameters. In order to properly describe the tails of the resolution, avoiding detector biases which occur when a Gaussian approximation is made, we use the explicit resolution histogram for signal and feed-down. The detector resolution is about 4 MeV/c^2, much smaller than the intrinsic width of the resonances, but the tails are significantly larger. On the other hand, Gaussian resolution is sufficient for the broad states, since the tails fall outside the fitting window. The accuracy of the simulation of the detector resolution has been tested in a control sample of D^0 and D^{*+}, whose natural width is negligible with respect to detector resolution. After taking the detector resolution into account using the above prescription, we measure a width smaller than 0.2 MeV/c^2 for all momentum ranges, and use this value as a conservative systematic error on the width due to tracking precision. If instead, the Gaussian approximation was made for the width, we then observed width and mass shifts of the order of a few MeV/c^2, much larger than the precision envisaged.

The fitting procedure has been tested on a Monte Carlo sample of fully simulated $D_1^0 \to D^{*+}\pi^-$, $D_2^{*0} \to D^{*+}\pi^-$, and $D_2^{*0} \to D^+\pi^-$ decays with three times the statistics of

TABLE II. Shift of the measured masses and widths of D_1^0 and D_2^{*0} and χ^2 probability P for different hypotheses of the broad state; allowing parameters to float in the fit, using the values published by FOCUS [11] or Belle [15], or forcing it to zero in the $D\pi$ channel. Mass shifts are in MeV/c^2 and probability in percent.

Model	$\Delta(M_{D_1^0})$	$\Delta(\Gamma_{D_1^0})$	$\Delta(M_{D_2^{*0}})$	$\Delta(\Gamma_{D_2^{*0}})$	$P(\chi^2)$
Free	...	...	...	...	51
FOCUS	0.1	0.2	0.1	0.5	50
Belle	0.1	0.3	0.1	0.5	50
Absent	0.1	0.4	0.1	0.6	52

the observed data. The feed-downs are also included. However, they have a small impact on the final result. Both background and broad-state events have been generated from the parametrized data distribution. With this sample, two important cross-checks on the fitting algorithm have been performed. First, the full simulation sample is fitted and the results agree with the simulation input parameters. In addition, a large number of "toy experiments" with statistics comparable to the data are generated and fit to look for potential biases. The resultant pull distribution for each fit parameter is consistent with a Gaussian distribution of zero mean and unit width.

The likelihood fit applied to the data yields roughly 7500 D_1^0 and 5000 D_2^{*0} candidates for the channel of Fig. 3 and 20 000 D_2^{*0} candidates for that of Fig. 4. Given the large background of unknown shape, there is no way to derive the presence of a broad state from our data only. Leaving all its parameters free, the resulting broad-state yield is small and the χ^2 quality of fit probability is 51%. Three additional hypotheses on the broad state are tested: a mass and width as measured by FOCUS [11], as measured by Belle [15], or omitting the BS term from the fit. The resulting variations in the measured quantities are shown in Table II. As the differences are small and there is no discrimination on the basis of the χ^2 probability, the central result includes the broad state with free parameters, and other options provide estimates of systematic uncertainty.

From the likelihood fit we derive results, with statistical uncertainties only, on the D_1^0 and D_2^{*0} widths and mass differences with respect to the D^{*+} or D^+ into which the D^{**} decays. To derive absolute masses from the measured mass differences we add the world average masses [24] of the D^{*+} or D^+, and the corresponding uncertainty on this value (both known with 0.5 MeV/c^2 precision) to the systematic errors. The remaining residual systematic errors are connected with Monte Carlo statistics and the tracking calibration, and are listed in Table III.

In summary, the large sample of orbitally excited charmed mesons collected by the CDF collaboration using the vertex trigger allows the measurement of properties of the $L = 1$ orbitally excited narrow states D_1^0 and D_2^{*0} with unprecedented precision. Using both $D^{*+}\pi^-$ and $D^+\pi^-$ final states, the measured widths of these states are

$$\Gamma(D_1^0) = 20.0 \pm 1.7 \pm 1.3 \text{ MeV}/c^2,$$
$$\Gamma(D_2^{*0}) = 49.2 \pm 2.3 \pm 1.3 \text{ MeV}/c^2,$$

where the first error is statistical, and the second systematic, above and for all results which follow. In order to improve the resolution, the mass measurement is performed in term of differences with respect to the daughter charmed particle. The measured mass differences are

TABLE III. Summary of systematic error for the mass and width of the two resonances, all in units of MeV/c^2. Since the measurement is a mass difference, the absolute mass error includes a systematic error due to the uncertainty of the mass of the reference particle.

Source	$\Delta(M_{D_1^0})$	$\Delta(\Gamma_{D_1^0})$	$\Delta(M_{D_2^{*0}})$	$\Delta(\Gamma_{D_2^{*0}})$
MC statistics	0.3	1.2	0.4	1.2
Broad state	0.1	0.4	0.1	0.5
Track error scale	0.1	...	0.1	...
Fit model	<0.1	<0.1	<0.1	<0.1
Mass calibration	0.1	0.2	0.1	0.2
Total (relative)	0.4	1.3	0.5	1.3
Reference mass	0.5	...	0.7	...
Total (absolute)	0.6	1.3	0.8	1.3

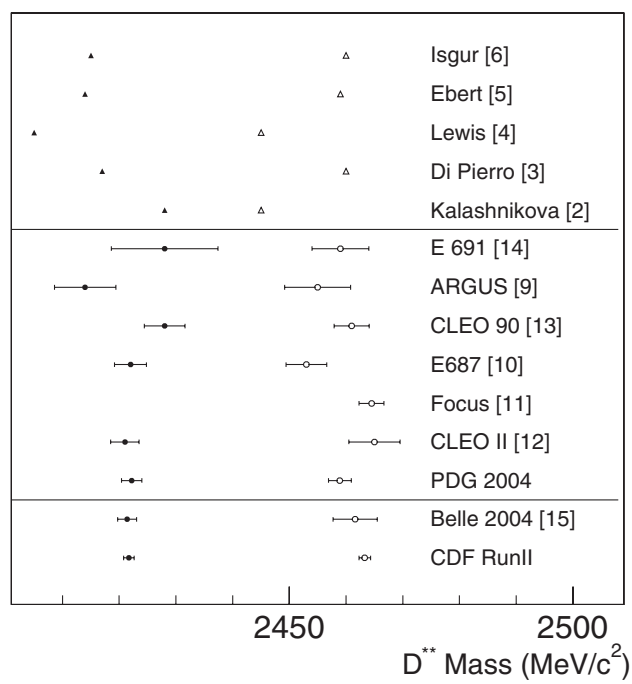

FIG. 5. D_1^0 (solid) and D_2^{*0} (open) mass comparison with theoretical expectations (triangles) and previous measurements and current world average (circles). Errors for theory predictions are not readily available.

$$M(D_1^0) - M(D^{*+}) = 411.7 \pm 0.7 \pm 0.4\ \mathrm{MeV}/c^2,$$
$$M(D_2^{*0}) - M(D^+) = 593.9 \pm 0.6 \pm 0.5\ \mathrm{MeV}/c^2.$$

The D_2^{*0} mass is given with respect to the D^+ since almost all the information comes from this decay channel. Adding the world average values for the D^{*+} and D^+ masses and including their uncertainties in quadrature to the systematic error, the absolute values of the masses are

$$M(D_1^0) = 2421.7 \pm 0.7 \pm 0.6\ \mathrm{MeV}/c^2,$$
$$M(D_2^{*0}) = 2463.3 \pm 0.6 \pm 0.8\ \mathrm{MeV}/c^2.$$

A comparison of these values with the world averages and some recent theoretical models can be found in Fig. 5; the results are consistent with the models, and with better estimations of uncertainties from the models they should allow one to constrain which theoretical picture is consistent with experiment. Comparison with predictions and measurements for the widths is less insightful due to the larger uncertainties; however, the width measurements presented here are consistent with other recent measurements [12,15].

This is the best single world measurement of the masses of the orbitally excited charm states. The total error is still limited by the statistics, and there is room for improvement with the data presently being recorded by the CDF II experiment. A precise determination of the theory uncertainties would however be needed to assess the discriminating power of this and future measurements.

We thank the Fermilab staff and the technical staffs of the participating institutions for their vital contributions. This work was supported by the U.S. Department of Energy and National Science Foundation; the Italian Istituto Nazionale di Fisica Nucleare; the Ministry of Education, Culture, Sports, Science and Technology of Japan; the Natural Sciences and Engineering Research Council of Canada; the National Science Council of the Republic of China; the Swiss National Science Foundation; the A.P. Sloan Foundation; the Bundesministerium für Bildung und Forschung, Germany; the Korean Science and Engineering Foundation and the Korean Research Foundation; the Particle Physics and Astronomy Research Council and the Royal Society, U.K.; the Russian Foundation for Basic Research; the Comisión Interministerial de Ciencia y Tecnología, Spain; in part by the European Community's Human Potential Programme under Contract No. HPRN-CT-2002-00292; and the Academy of Finland.

[1] N. Isgur and M. Wise, Phys. Lett. B **232**, 113 (1989); **237**, 527 (1990).
[2] A. F. Falk and M. E. Peskin, Phys. Rev. D **49**, 3320 (1994).
[3] Y. S. Kalashnikova and A. V. Nefediev, Phys. Lett. B **530**, 117 (2002).
[4] M. Di Pierro and E. Eichten, Phys. Rev. D **64**, 114004 (2001).
[5] R. Lewis and R. M. Woloshyn, Phys. Rev. D **62**, 114507 (2000).
[6] D. Ebert, V. O. Galkin, and R. N. Faustov, Phys. Rev. D **57**, 5663 (1998); AIP Conf. Proc. **619**, 336 (2002).
[7] N. Isgur, Phys. Rev. D **57**, 4041 (1998).
[8] S. Godfrey and N. Isgur, Phys. Rev. D **32**, 189 (1985); S. Godfrey and R. Kokoski, Phys. Rev. D **43**, 1679 (1991).
[9] H. Albrecht *et al.* (ARGUS Collaboration), Phys. Lett. B **232**, 398 (1989).
[10] P. L. Frabetti *et al.* (E687 Collaboration), Phys. Rev. Lett. **72**, 324 (1994).
[11] J. Link *et al.* (FOCUS Collaboration), Phys. Lett. B **586**, 11 (2004).
[12] P. Avery *et al.* (CLEO Collaboration), Phys. Lett. B **331**, 236 (1994).
[13] P. Avery *et al.* (CLEO Collaboration), Phys. Rev. D **41**, 774 (1990).
[14] J. C. Anjos *et al.* (E691 Collaboration), Phys. Rev. Lett. **62**, 1717 (1989).
[15] K. Abe *et al.* (BELLE Collaboration), Phys. Rev. D **69**, 112002 (2004).
[16] V. M. Abazov *et al.* (D0 Collaboration), Phys. Rev. Lett. **95**, 161602 (2005).
[17] D. Acosta *et al.* (CDF Collaboration), FERMILAB Report No. FERMILAB-PUB-96/390-E, 1996; Phys. Rev. D **68**, 072004 (2003).
[18] CDF uses a cylindrical coordinate system (r, ϕ, z) with the origin at the center of the detector and the positive z direction aligned with the proton direction. Psuedorapidity η is defined as $\eta \equiv -\ln(\tan(\theta/2))$, where θ is the polar angle.
[19] A. Sill *et al.*, Nucl. Instrum. Methods Phys. Res., Sect. A **447**, 1 (2000).
[20] T. Affolder *et al.*, Nucl. Instrum. Methods Phys. Res., Sect. A **526**, 249 (2004).
[21] E. J. Thomson *et al.*, IEEE Trans. Nucl. Sci. **49**, 1063 (2002).
[22] W. Ashmanskas *et al.*, Nucl. Instrum. Methods Phys. Res., Sect. A **447**, 218 (2000).
[23] D. Acosta *et al.* (CDF Collaboration), hep-ex/0508022.
[24] S. Eidelman *et al.* Phys. Lett. B **592**, 1 (2004).